Decadal increase in Arctic dimethylsulfide emission

Martí Gali[a,1,2], Emmanuel Devred[b], Marcel Babin[a,c], and Maurice Levasseur[a]

[a]Takuvik Joint International Laboratory (Université Laval), Biology Department, Université Laval, Québec, QC, G1V 0A6, Canada; [b]Fisheries and Oceans Canada, Bedford Institute of Oceanography, Dartmouth, NS, B2Y 4A2, Canada; and [c]Takuvik Joint International Laboratory (CNRS, France), Biology Department, Université Laval, Québec, QC, G1V 0A6, Canada

Edited by David M. Karl, University of Hawaii at Manoa, Honolulu, HI, and approved July 30, 2019 (received for review March 13, 2019)

Dimethylsulfide (DMS), a gas produced by marine microbial food webs, promotes aerosol formation in pristine atmospheres, altering cloud radiative forcing and precipitation. Recent studies suggest that DMS controls aerosol formation in the summertime Arctic atmosphere and call for an assessment of pan-Arctic DMS emission (EDMS) in a context of dramatic ecosystem changes. Using a remote sensing algorithm, we show that summertime EDMS from ice-free waters increased at a mean rate of 13.3 ± 6.7 Gg S decade^{-1} (~33% decade^{-1}) north of 70°N between 1998 and 2016. This trend, mostly explained by the reduction in sea-ice extent, is consistent with independent atmospheric measurements showing an increasing trend of methane sulfonic acid, a DMS oxidation product. Extrapolation to an ice-free Arctic summer could imply a 2.4-fold (±1.2) increase in EDMS compared to present emission. However, unexpected regime shifts in Arctic geo- and ecosystems could result in future EDMS departure from the predicted range. Superimposed on the positive trend, EDMS shows substantial interannual changes and nonmonotonic multiyear trends, reflecting the interplay between physical forcing, ice retreat patterns, and phytoplankton productivity. Our results provide key constraints to determine whether increasing marine sulfur emissions, and resulting aerosol–cloud interactions, will moderate or accelerate Arctic warming in the context of sea-ice retreat and increasing low-level cloud cover.

dimethylsulfide | Arctic Ocean | plankton | sea ice | aerosols

The Arctic region is warming more than 2 times faster than the global average, and ice-free summers could be a reality in the next few decades (1). Removal of the ice barrier boosts ocean–atmosphere exchanges of energy, gases, and particles, with profound effects on marine ecosystems and climate. Enhanced heat and moisture fluxes are increasing the abundance of low-level clouds (2) and, very likely, the prevalence of liquid-state clouds and precipitation (3). Ice retreat allows more solar radiation to penetrate into the ocean surface, driving a pan-Arctic increase in phytoplankton primary production (2, 4–6). Meanwhile, changes in stratification and nutrient supply to the sunlit ocean layer modulate phytoplankton productivity (4–7) and alter phytoplankton bloom phenology (7–10) and the occurrence of species with distinct biogeochemical traits (10–12) such as their capacity to produce the climate active gas dimethylsulfide (DMS) (13, 14). DMS is produced through microbial decomposition of dimethylsulfoniopropionate (DMSP), a compound synthesized in variable amounts by different phytoplankton groups (13, 14). Despite complex biogeochemical cycling (14, 15), high-latitude DMS production scales to first order with phytoplankton biomass and productivity over the seasonal cycle at large scales (16–19). In a scenario of changing ice cover and phytoplankton dynamics, changes in the magnitude, timing, and spatial distribution of Arctic DMS emission (EDMS) are expected (14, 20, 21).

Previous estimates of Arctic Ocean EDMS have been made using either sea-surface DMS climatologies (16), produced through interpolation of sparse in situ data, or prognostic models (20, 21). Both types of estimates depict the Arctic as a region with relatively low sea–air DMS flux per unit area (FDMS) on an annual basis (mean FDMS lower than 2 μmol m^{-2}·d^{-1}) compared to temperate and tropical oceans (mean FDMS of about 4–5 μmol m^{-2}·s^{-1}) (16, 20). However, Arctic FDMS is concentrated in the short productive summer season, and relatively high daily fluxes have been reported associated with phytoplankton blooms that form in the wake of melting sea ice, often exceeding 10 μmol m^{-2}·s^{-1} (14, 15). Ice margin phytoplankton blooms are a major feature of the Arctic ecosystem. They typically last for 1–3 wk after ice breakup and are promptly detected using ocean color remote sensing (8, 9, 22). Given the patchy and ephemeral nature of Arctic EDMS, accurate estimates of its magnitude and spatial–temporal distribution based on climatological datasets are severely limited.

Once emitted to the atmosphere, the influence of DMS on atmospheric particles does not depend strictly on the magnitude of FDMS. Rather, it is the background concentration of aerosol particles that critically determines whether atmospheric DMS oxidation products can nucleate new particles or condense onto preexisting ones (23–25). In summer, different processes isolate the Arctic marine boundary layer from southern aerosol sources (both natural and anthropogenic), namely: the northward migration of the atmospheric polar front, the efficient wet scavenging by drizzling stratocumulus clouds, and the formation of surface inversion layers (3, 25, 26). These processes result in extremely low aerosol concentrations, which favor new particle formation from local gaseous precursors (23, 25, 27, 28). Recent measurements and associated modeling have shown instances where DMS controls the formation of ultrafine particles (23, 28), which can grow large enough to act as cloud condensation nuclei (CCN) (23, 25). Thus, changes in Arctic Ocean EDMS could alter aerosol populations, light scattering, and cloud-seeding activity (26, 27, 29,

Significance

As Arctic sea-ice cover declines because of climate warming, the emission of reactive gases produced by marine microbes increases. One of such gases, dimethylsulfide, forms new atmospheric particles that contribute to cloud formation. This can either cool the Earth's surface by reflecting incoming sunlight, or warm it due to the blanket effect. Here we quantify Arctic Ocean dimethylsulfide emission between 1998 and 2016 using satellite observations of microalgal biomass and physical variables. We report an increasing trend, driven by sea-ice loss, and substantial year-to-year variability modulated by biological productivity. Our results can help understand the impacts and feedbacks of marine plankton on Arctic climate and foresee their future trajectories under the pressure of global change.

Author contributions: M.G., M.B., and M.L. designed research; M.G. and E.D. performed research; M.G. analyzed data; and M.G., E.D., M.B., and M.L. wrote the paper.

The authors declare no conflict of interest.

This article is a PNAS Direct Submission.

Data deposition: The DMSSAT algorithm code has been deposited in GitHub (https://github.com/mgali/), and curated in situ datasets and DMSSAT datasets have been deposited at Zenodo (https://doi.org/10.5281/zenodo.3243967).

[1]Present address: Earth Sciences Department, Barcelona Supercomputing Center, 08034 Barcelona, Spain.

[2]To whom correspondence may be addressed. Email: marti.gali.tapias@gmail.com.

This article contains supporting information online at www.pnas.org/lookup/suppl/doi:10.1073/pnas.1904378116/-/DCSupplemental.

First published September 9, 2019.

30), and hence the capacity of clouds to reflect incoming radiation (shortwave forcing or albedo) and trap heat (longwave forcing) (3, 24, 31–33).

To document trends in EDMS in the Arctic, we calibrated for high northern latitudes the DMS_{SAT} algorithm (17), which estimates sea-surface DMS concentration (nM) from remotely sensed variables, chiefly chlorophyll *a* concentration (Chl), light penetration depths, and photosynthetically available radiation. We implemented and validated the algorithm at 8-d and 28-km resolution, covering a total of 19 y using data from 2 sensors: the Sea-viewing Wide Field-of-view Sensor (SeaWiFS, years 1998–2007), and the Moderate Resolution Imaging Spectroradiometer onboard the Aqua satellite (MODIS-Aqua, 2003–2016) (34). This enables the exploration of interannual changes and trends in EDMS from ice-free Arctic and Subarctic waters.

Results and Discussion

DMS Concentration and Emission Patterns in Northern High Latitudes. The satellite algorithm shows remarkable skill across 2 orders of magnitude of DMS concentration when compared to in situ data, with $\log_{10}$ space root-mean-square error of 0.40 and Pearson's correlation coefficient of 0.64 (*SI Appendix*, Fig. S3). Comparison between DMS_{SAT} results and the existing climatology based on interpolation of in situ DMS data (16) (here referred to as L11) highlights the strengths of the satellite algorithm. In areas with little or no seasonal ice cover, including 3 distinct ecoregions in the North Atlantic (50°N-80°N; Fig. 1 *C*–*E*) and the Bering Sea (Fig. 1*G*), the mean DMS_{SAT} seasonal cycle agrees well with L11. Good agreement between DMS_{SAT} and L11 is also found for the whole study domain (latitudes >50°N; Fig. 1*B*). In contrast, in the seasonal ice zone, temporal (Fig. 1 *F* and *H*) and spatial (*SI Appendix*, Fig. S4) patterns derived from DMS_{SAT} differ markedly from the L11 climatology. In these areas, satellite-derived DMS reflects elevated concentrations (often ≥5 nM) in the wake of melting sea ice, in better accordance with several field surveys of phytoplankton blooms in the marginal ice zone (14, 15, 35). Another salient feature of DMS_{SAT} results is the wide interannual variability in the magnitude and timing of maximal DMS concentrations (Fig. 1 *C*–*H*). None of these features can be examined using global DMS climatologies, produced through multiyear averaging, interpolation, and smoothing of sparse in situ measurements (16, 17).

We calculated sea–air DMS flux (FDMS; μmol S $m^{-2}{\cdot}d^{-1}$), for ice-free waters only (<10% ice cover per pixel), using satellite DMS fields, meteorological reanalysis data, and gas-exchange parameterizations (*SI Appendix*, Fig. S5). Here, we examine large-scale FDMS patterns during the summer period, defined as May to August (year days 121–248), when ∼70% of the annual open-water emission occurs. As shown in Fig. 2*A*, the main feature of FDMS is a marked decrease between 55°N and 80°N. This reflects the combination of 3 main controlling factors, all of which decrease poleward: 1) the duration of the ice-free season (4), 2) the mean summertime DMS concentration (*SI Appendix*, Fig. S4), and 3) the sea–air gas transfer coefficient (K_w), which in turn depends on wind speed and sea-surface temperature (SST) (*SI Appendix*, Fig. S5). Compared to subarctic seas, the Arctic seasonal ice zone stands out as a region of overall low summer-integrated FDMS (Fig. 2*B*), concentrated during a brief period (contour lines in Fig. 2*C*) when FDMS can be locally high but also variable (*SI Appendix*,

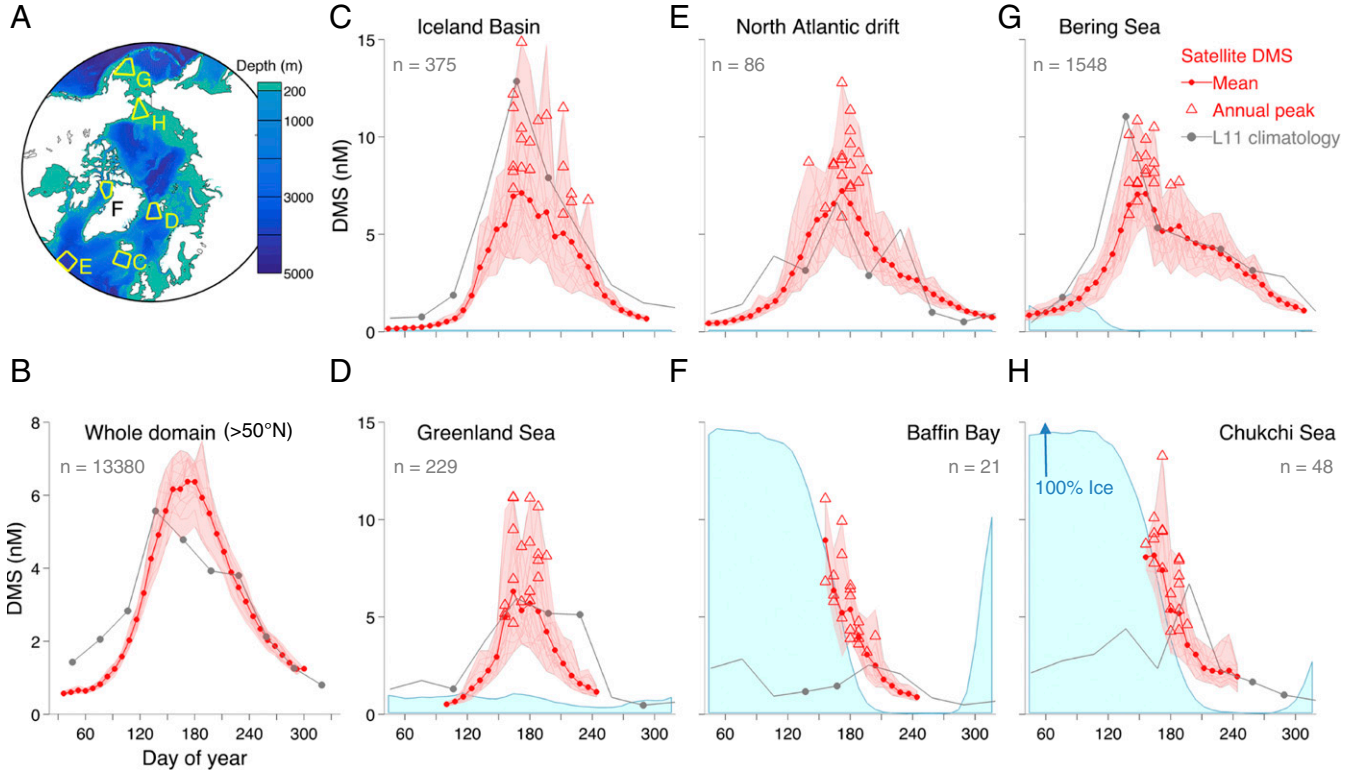

Fig. 1. DMS seasonal cycles in Subarctic and Arctic seas. (*A*) Bathymetric map and ecoregions (yellow polygons) used to illustrate DMS dynamics; (*B*–*H*) mean DMS seasonal cycle derived from the satellite algorithm (red line and dots) and from the L11 climatology (gray line and dots) for latitudes higher than 50°N (*B*) and 6 smaller ecoregions (*C*–*H*) shown in *A*. In the satellite seasonal cycles (*C*–*H*), light-red lines mark individual years, light-red shadow marks the 19-y envelope, and red triangles mark the annual peak for each year. In the monthly L11 climatology, markers indicate that in situ data were available in a given month, whereas no marker indicates that monthly DMS was estimated through interpolation. The numbers in gray indicate the amount (n) of in situ measurements available to calculate the L11 climatology in a given ecoregion (1979–2010). The light-blue shade is the mean fractional ice cover, scaled to the maximum of the *y* axis, shown only for regions within the seasonal ice zone. Analogous plots for FDMS are shown in *SI Appendix*, Fig. S6.

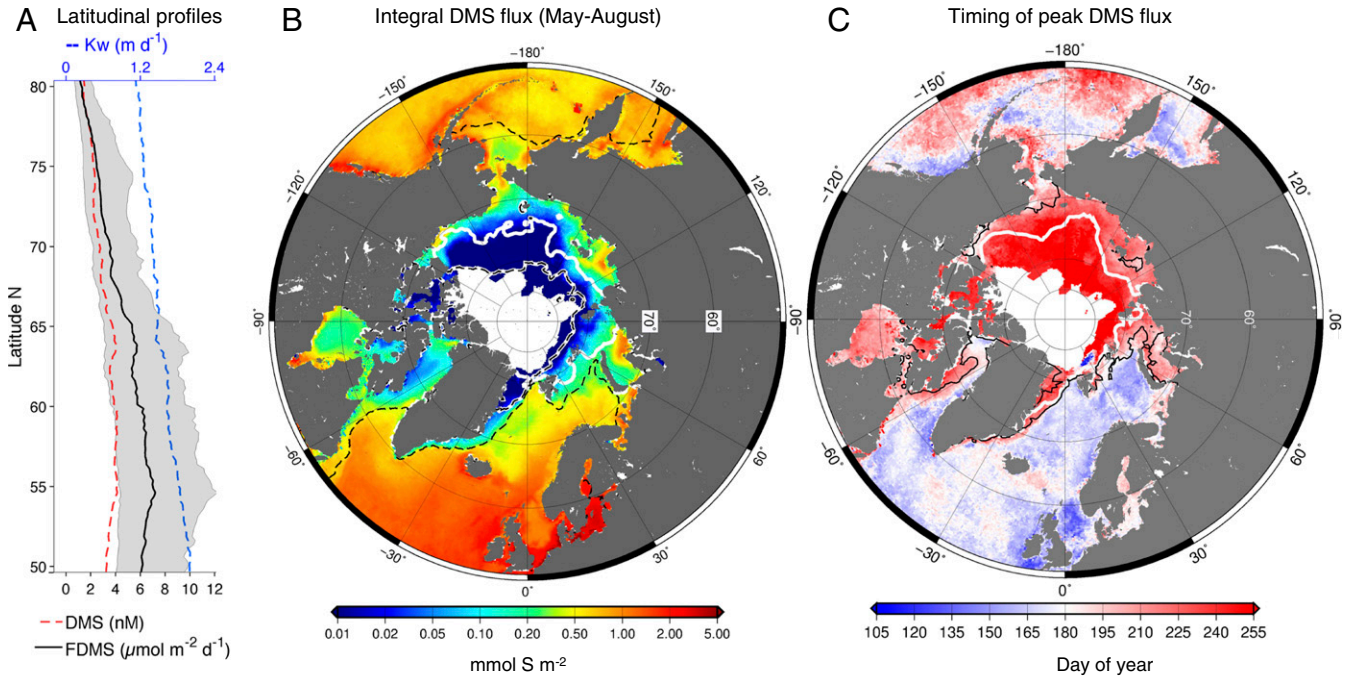

Fig. 2. Spatial distribution and timing of summertime DMS emission in May through August 2003–2016. (*A*) Median latitudinal profile in ice-free pixels of sea-surface DMS concentration, sea–air flux (FDMS; interquartile range is shaded), and sea–air gas-exchange coefficient (K_w); (*B*) integral summertime FDMS between year days 121 and 248; (*C*) mean day of the annual peak in sea–air DMS flux. Contour lines in *B* show: 2003–2016 median of maximal late winter ice extent (black dashed line); minimal early September ice extent in 2003 (white line); minimal early September ice extent in 2012 (black dashed on white line). Contours in *C* enclose the area where: more than 50% of the summertime DMS emission occurs during a 24-d period centered on the annual peak (black line); the duration of the ice-free season is shorter than 48 d (white line) (medians of the 2003–2016 period).

Fig. S6). The frequency of FDMS >10 μmol $m^{-2}{\cdot}d^{-1}$ based on satellite diagnosed DMS is 3-fold higher than that based on L11 (*SI Appendix*, Fig. S6) and, unlike the latter, can reach up to 30 μmol $m^{-2}{\cdot}d^{-1}$, in agreement with in situ studies (15, 35).

Pan-Arctic Summer DMS Emission, 1998–2016. To estimate DMS emission (EDMS), we integrated FDMS over latitudinal and bathymetric domains through the summer (May–August) period. The mean satellite-based EDMS in summer between years 1998 and 2016 was 113 ± 10 and 50 ± 11 Gg S for the 60–70°N and >70°N latitude bands, respectively (Fig. 3). These estimates are robust to uncertainty in satellite input data and algorithm coefficients (*SI Appendix*, Table S3).

Satellite-derived time series indicate that Arctic summer EDMS increased significantly between 1998 and 2016 (Fig. 3). The 70–75°N and 75–80°N latitude bands contributed most of the increase, with about 6 Gg S $decade^{-1}$ each (Fig. 3). In relative terms, however, this implies a faster increase in the 75–80°N band (74% $decade^{-1}$) compared to the 70–75°N band (21% $decade^{-1}$), with respect to the 1998–2003 baseline. A very small but significant trend of 0.36 ± 0.15 Gg S $decade^{-1}$ is detected north of 80°N, which nonetheless corresponds to more than a doubling per decade. The total rate of increase of summer EDMS, north of 70°N, is 13.3 ± 6.7 Gg S $decade^{-1}$, or 33 ± 17% $decade^{-1}$ (Fig. 4*A*). The months of June and July dominate this response (8.3 ± 4.3 Gg S $decade^{-1}$). Interestingly, the positive trend north of 70°N was accompanied by a smaller nonsignificant decrease between 60°N and 70°N of −5.4 ± 8.4 Gg S $decade^{-1}$ (−4.8 ± 7.5% $decade^{-1}$) (Fig. 3). Altogether, this reveals a poleward shift of DMS emissions.

Hitherto, the only evidence for increasing Arctic Ocean EDMS came from atmospheric measurements of methane sulfonic acid (MSA), a specific product of DMS oxidation. In 3 Arctic stations (Barrow, Alaska; Alert, Nunavut; Mt. Zeppelin, Svalbard), MSA concentration in aerosol samples increased at a rate of between 45 and 83% $decade^{-1}$ between 1998 and 2009 during July and August (30), concomitant with pronounced sea-ice loss north of 70°N. Our satellite-derived EDMS estimates for the same period and months suggest an increase of 40% $decade^{-1}$ north of 70°N, at the lower bound of MSA rates of increase. Note however that our assessment does not include ice-infested waters, sea-ice microorganisms, and melt ponds, whose EDMS could also be increasing (14). Although ice-free seawater largely dominates present-day EDMS (36, 37), better knowledge of ice-related and nonmarine DMS sources is needed (37). Yet, the overall consistency between our satellite estimates and independent MSA measurements lends confidence to the observed EDMS trends.

Ice Retreat Patterns and Ocean Productivity Control Arctic EDMS. The 19-y EDMS time series shows 3 distinct periods and a nonmonotonic behavior (Fig. 4*A*). EDMS showed small oscillations between 1998 and 2003, increased rapidly between 2003 and 2011, and decreased at a similar rate between 2011 and 2016. Between 2003 and 2011, EDMS increased by 111%, more than expected from the increase in ice-free extent alone (39%; Fig. 4*B*), due to a concomitant increase in mean FDMS (55%; Fig. 4*C*); heightened FDMS reflected, in turn, slight increases in DMS and K_w in open waters. Conversely, EDMS decreased between 2011 and 2016 owing to decreased DMS concentration in open waters, although ice-free extent showed erratic oscillations and K_w continued to increase slowly (Fig. 4 *E*–*G*).

The ice-free ocean extent in summer north of 70°N increased between 1998 and 2016 at a mean rate of 28 ± 7% per decade, with a maximum in 2012 (Fig. 4*B*). This trend is similar to the mean rate of increase in EDMS (33% $decade^{-1}$) and explains 68% of its interannual variance (Fig. 4*I*). To appraise the effect of seawater DMS variability on EDMS variability at the interannual timescale, we recomputed EDMS replacing the 19-y DMS_{SAT} time series by climatological DMS fields, while allowing sea ice, wind

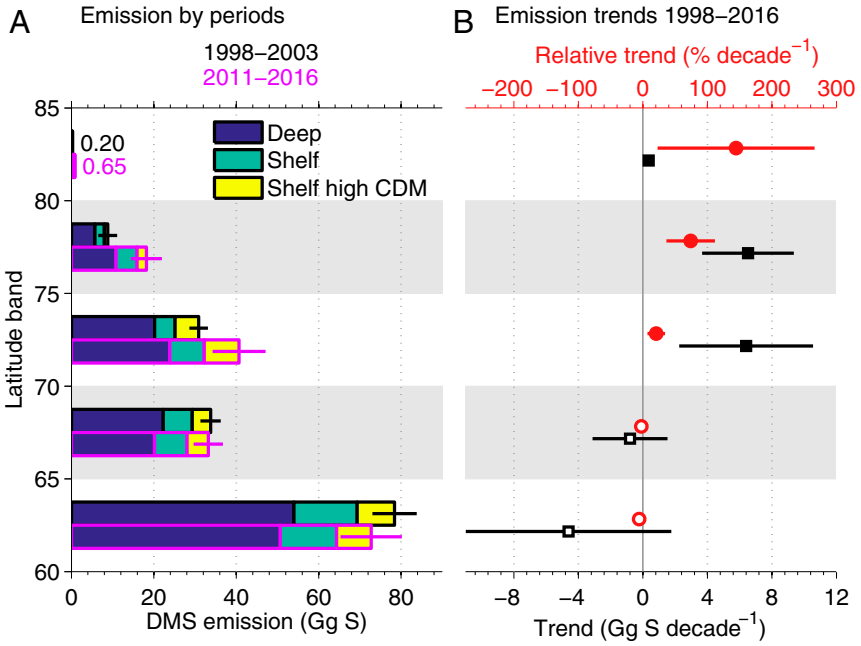

Fig. 3. Mean zonal trends in summertime (May–August) EDMS. (*A*) EDMS mean ± SD for 1998–2003 (black line) and 2011–2016 (gray line); emissions are broken down into deep-ocean basins and continental shelves. The latter are further divided to show waters with strong riverine influence as depicted by high content of CDM that increases uncertainty in satellite Chl retrievals. (*B*) EDMS trends for the period 1998–2016 (black squares), and corresponding relative increase with respect to the 1998–2003 baseline period (red circles). Filled symbols mark significant trends at 95% confidence level, and error bars show the SE of the linear regression slope (which is sometimes smaller than the symbols).

speed, and SST to vary. In this experiment, the fraction of EDMS variance explained by ice-free extent increased from 68 to 87% (89%) using the DMS_{SAT} (L11) 8-d climatology. This exercise shows that changes in sea-surface DMS concentration (reflecting underlying ecosystem productivity) cause substantial interannual variability in FDMS and therefore in EDMS, adding to the variability arising from gas-exchange coefficients (Fig. 4 *E*–*G*). To further explore the interplay between ice cover and FDMS, we performed a spatial decomposition of EDMS changes over successive years (*SI Appendix*, Fig. S7). This analysis shows that net changes in ice-free extent and shifts in ice retreat patterns over the melt season dominated interannual changes in EDMS. Yet, local FDMS variations contributed similarly to EDMS changes in some years, especially after 2010.

Since the Arctic Ocean comprises contrasting biogeochemical regimes (2, 4, 6, 7), regional breakdown is needed to understand the interplay between the geographic patterns of ice retreat and the drivers of EDMS. Our analysis indicates that interannual EDMS changes result from 2 main components (Fig. 4). On one hand, the Atlantic-influenced Greenland and Barents Seas, with low or moderate ice cover, moderate productivity, and relatively high wind speed and SST (hence K_w), generally dominated EDMS north of 70°N. These Atlantic-influenced seas displayed modest interannual variability and a smaller-than-average positive EDMS trend (19 ± 10% decade^{-1} between 1998 and 2016). On the other hand, inner Arctic shelves displayed wider variability and trends, particularly the Kara and Laptev Seas, owing to the convolution of large variations in ice-cover distribution and sharper FDMS gradients (Fig. 2*B*). Extreme expression of this pattern occurred in 2003 and 2011, as illustrated with pie charts in Fig. 4. In 2003 the Atlantic sector dominated EDMS, whereas in 2011 the inner shelves dominated EDMS despite the concurrent increase in Atlantic sector emissions (*SI Appendix*, Fig. S8).

Modulation of Arctic EDMS by the interplay between variable ice retreat and sea-surface DMS patterns is a salient finding enabled by satellite remote sensing. The magnitude of FDMS-driven interannual variability reported here should be viewed with caution due to 1) the lack of multiyear in situ DMS time series across Arctic ecoregions, and 2) increased DMS_{SAT} uncertainty in river outflow areas, mainly caused by uncertainty in satellite chlorophyll (note however that river outflow areas account for a minor fraction of pan-Arctic EDMS; Fig. 3*A*) (*SI Appendix*, section 5). Despite these shortcomings, the temporal trends and spatial patterns we observe are broadly consistent with those previously reported for satellite-based primary production between 1998 and 2012 (4, 6, 9) (which suffer from similar uncertainties as DMS_{SAT}). In summary, our results suggest that the Arctic Ocean will display substantial interannual variability and periods of transient EDMS decrease, superimposed on the robust upwards EDMS trend dictated by ice receding (Fig. 4*I*), during its transition to an ice-free state in summer.

Future Scenarios. Can contemporary changes hint at the future Arctic Ocean EDMS? Extrapolation of our results to a 100% ice-free Arctic in summer implies a 2.4-fold increase in EDMS (1.2–3.6, propagated 95% confidence interval, CI) with respect to the 2011–2016 average, and a mean summertime EDMS of 144 ± 66 Gg S north of 70°N (Fig. 4*I*). New emissions are expected to arise mostly from regions that presently have relatively high ice cover, namely the productive inner Arctic shelves. Conversely, the Atlantic sector, with low or moderate ice cover at present, is close to attaining its full EDMS potential if FDMS remains at current levels. Previous projections of EDMS suggested an increase of between 2- and 15-fold in an ice-free Arctic, and were largely sensitive to the representation of sea-surface DMS concentrations (see compilation in *SI Appendix*). Our satellite-based assessment, which accounts for domain-specific responses, helps constraining these projections and suggests that an increase larger than 3-fold is unlikely. This is because complete sea-ice loss from the Central Arctic basin, with heavy ice cover at present, will contribute little new EDMS due to prevailing low FDMS in satellite-observed pixels in that area (Fig. 2*B*).

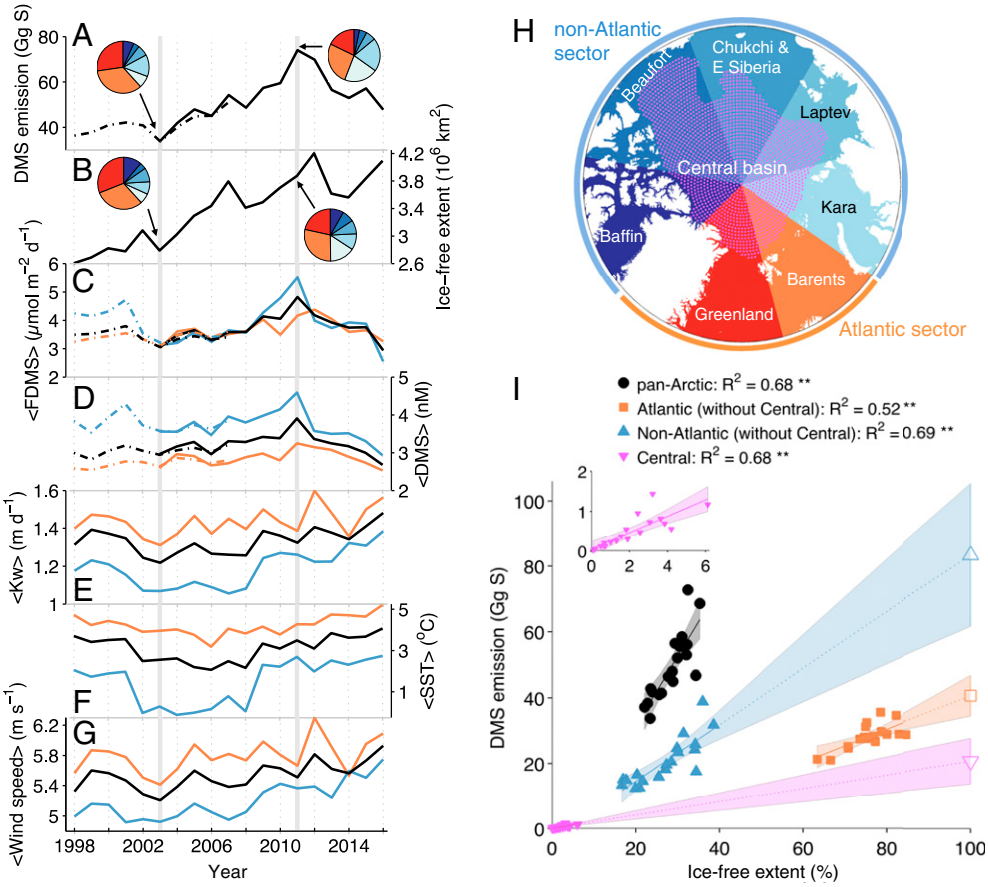

Fig. 4. Interannual variations in EDMS and its driving factors north of 70°N. All panels show May–August integrals (EDMS) or means (other variables). (*A*) EDMS, (*B*) mean ice-free ocean extent, (*C*) mean FDMS, (*D*) mean DMS concentration, (*E*) sea–air DMS transfer coefficient (K_w), (*F*) SST, (*G*) wind speed. Values in *C*–*G* correspond to ice-free pixels only. Different lines correspond to the whole domain >70°N and its division into 2 sectors: Atlantic-influenced and non-Atlantic regions, according to the map in *H*. The pie charts in *A* and *B* illustrate the relative contribution of different source regions (colored following *H*) to EDMS, and their corresponding share of ice-free extent, in the years with lowest (2003) and highest (2011) EDMS. (*I*) shows the domain-specific relationship between % ice-free extent and EDMS. In this plot, the Central Arctic basin (pink stippling in *H*) is treated separately, and its area subtracted from the other regions to calculate the regressions (the regression for the Central basin is also shown in the *Inset*). Empty symbols show extrapolation to 100% ice-free extent for the Atlantic, non-Atlantic, and Central domains, and shaded areas show the 95% CI of predictions.

The scenario described above is consistent with conceptual (7) and numerical (5) model predictions suggesting that salinity stratification and resulting nutrient limitation will prevent large increases in phytoplankton production in the Arctic as sea-ice loss proceeds. However, our EDMS estimates for an idealized ice-free scenario suffer from multiple sources of uncertainty. First, the observed linear relationship between ice-free extent and EDMS will not necessarily hold in the future, and its extrapolation is particularly speculative in domains with high ice cover at present (Fig. 4*I*). Second, estimation of future EDMS is confounded by additional layers of complexity that interact with each other (14): the response of plankton communities to multiple stressors, with a potentially prominent but poorly understood role for acidification (38); the strong taxonomic dependence of DMSP synthesis; and the complex biogeochemical cycling of DMS in seawater (13, 14).

The relationship between airborne MSA and phytoplankton production in historical records could help constrain EDMS projections (14, 18, 19). MSA trapped in Greenland ice cores shows a robust positive relationship with in situ sampled phytoplankton and satellite-observed net primary production (NPP) around southern Greenland over several decades (19). This observation supports extrapolation of the satellite-era EDMS trends. Yet, the relationship between NPP and MSA may be confounded by variable atmospheric MSA yields (14, 30) and by differences in phytoplankton taxonomy across source regions (18, 36). In the light of these findings, the response of Arctic phytoplankton to environmental forcing appears particularly critical. A warmer, more stable, and irradiated water column (7, 15) might favor nanoplanktonic strong DMS producers, like coccolithophores (10) and *Phaeocystis pouchetii* (20). Such a taxonomic shift could enhance EDMS from the seasonal ice zone, offsetting other processes suspected to affect negatively EDMS, e.g., acidification (38).

Understanding and predicting how changes in marine EDMS will affect the Arctic climate requires progress in many fronts. Although atmospheric models still strive to represent aerosol (24, 26) and cloud (3, 33) dynamics, there is growing consensus that 1) DMS is an essential ingredient for Arctic marine boundary layer nucleation; and 2) nucleation rates will increase in the future (3, 24, 26) owing to concomitant increases in atmospheric humidity, aerosol wet removal, and marine aerosol precursor emissions. In line with these predictions, increasing frequency of aerosol nucleation events has been clearly linked to ice retreat at the Mt. Zeppelin observatory (78.9°N) (27).

Current knowledge suggests that CCN concentrations are unlikely to increase as much as new particle formation (nucleation) rates, due to a concomitant increase in aerosol removal (24, 26). Yet, DMS will still play a critical role in seeding and sustaining CCN populations, and could also affect precipitation (26, 39). Widening the focus, the impact of increasing EDMS on CCN populations will also depend on changing anthropogenic sulfur

emissions and their transport to the Arctic. Ongoing reductions in power plant emissions in the Northern Hemisphere (40) may magnify the role of DMS or extend its seasonal dominance, unless they are compensated by increasing shipping, industrialization, or oil and gas extraction in the Arctic.

The future response of cloud radiative forcing is also uncertain. Unlike in lower latitudes, low-level marine clouds in the Arctic act to retain heat in the ocean–atmosphere system during most of the year (31). Net cloud cooling is currently restricted to a short midsummer period when high solar elevation and low ice cover cooccur, but the seasonal radiation budget will change as ice recedes. Extremely low CCN concentrations that generally occur over the ice pack imply strong sensitivity to CCN changes (32), amplifying uncertainty in indirect aerosol forcing (33). An increase in CCN concentrations is generally associated with enhanced cloud albedo and a cooling effect (3, 29, 33), with recent estimates suggesting a shortwave forcing of −1 to −2 W m^{-2} in response to a 2- to 5-fold increase in Arctic EDMS (3) (*SI Appendix*). However, a CCN increase might also enhance longwave cloud forcing over the CCN-depleted pack ice (32). This response is poorly quantified and could offset shortwave forcing, causing net warming and further accelerating ice melt (25, 27).

Our study highlights the key role of atmospheric forcing in driving Arctic EDMS through the control of ice retreat (41), plankton dynamics (7, 14), and gas exchange. Since large-scale weather systems also determine air-mass transport pathways (25), the fate of atmospheric DMS and its interaction with aerosols and clouds cannot be fully understood by analyzing climatological fields in the variable and heterogeneous Arctic environment. The space- and time-resolved FDMS estimates presented here provide a key constraint for atmospheric models and can help reduce uncertainty in projections of aerosol direct and indirect forcing (3, 24, 26, 33). This can in turn improve our understanding of contemporary plankton-climate feedbacks through the interaction of multiple processes, including ocean–atmosphere exchange of CO_2, other greenhouse gases, and aerosol precursors such as DMS (29, 38). Changing EDMS has wide implications for the vulnerable Arctic environment, its human populations, and the weather and climate of lower latitudes (1).

Methods

Remote Sensing Algorithms. Daily level 3 composites of remote sensing reflectance spectra acquired by SeaWiFS and MODIS-Aqua were used to retrieve Chl and euphotic layer depth (Zeu) [along with absorption coefficients of colored detrital matter ($a_{CDM}(412)$)]. These data were used as input to the DMS_{SAT} algorithm (17). First, sea-surface DMSPt (nmol L^{-1}) was estimated as a function of chlorophyll *a* (Chl) concentration using 2 different equations depending on the phytoplankton light exposure regime. Second, sea-surface DMS concentration (nmol L^{-1}) was estimated from DMSPt and photosynthetically available radiation, after binning these variables to 8-d 28-km resolution to achieve full coverage. Remotely sensed sea-ice concentration (SIC) was used to screen out ice-contaminated pixels (SIC > 10%). DMS_{SAT} was calibrated and validated for the Arctic region using in situ DMS and DMSPt data from a public database supplemented with recent datasets. DMS_{SAT} match-ups with in situ DMS yielded similar validation statistics for SeaWiFS and MODIS-Aqua. Detailed information on algorithm tuning, implementation, and validation is provided in *SI Appendix*.

DMS Sea–Air Flux. FDMS was estimated as the product of the sea–air gas transfer coefficient (K_w) and the DMS gradient across the sea–air interface using standard gas-exchange parameterizations based on wind speed. We took into account air- and water-side resistance and the effects of SST and salinity on DMS diffusivity and solubility (*SI Appendix*, section 4).

Large-Scale EDMS. We estimated EDMS by integrating FDMS over different periods and spatial domains (e.g., zonal bands and longitude sectors). The 200-m isobath was used to partition EDMS into open-ocean and continental shelf domains. Within continental shelves, a threshold of colored detrital matter $a_{CDM}(412) > 0.25$ m^{-1} was used to screen for riverine influence. High Arctic summer EDMS, defined as the May–August emission north of 70°N, was further regionalized into 7 longitude sectors (Fig. 4*H*). The Greenland and Barents Seas and the remaining 5 sectors were grouped into the Atlantic and non-Atlantic domains, respectively.

Relationship Between Ice Cover and EDMS. We computed linear least-squares regressions between EDMS and the percentage of open-ocean water (pixels with ≤10% SIC) for the high Arctic (>70°N) and for 3 domains within it: the Atlantic sector, the non-Atlantic sector, and the Central Arctic basin. Extrapolation to 100% ice-free water gave an estimate of future EDMS within a given domain, and the sum of extrapolated quantities gave a pan-Arctic estimate of future EDMS (Fig. 4*I*). Extrapolation based on the regression over the entire domain (which yielded 200 ± 54 Gg S, larger than the sum of domain-specific EDMS estimates) was discarded owing to uneven ice-free extent (%) and mean FDMS across domains. Uncertainty in future EDMS was propagated by adding in quadrature the 95% CI of the extrapolated predictions for each domain. Uncertainty in the fold change with respect to present-day EDMS also took into account the uncertainty in present-day EDMS estimates (2 SDs of 2011–2016 mean EDMS). Slopes obtained from alternative types of regression (type II major axis) were not significantly different from those obtained from regular linear least squares. Additional regressions between EDMS and ice-free extent (million km^2) in smaller longitude sectors are shown in *SI Appendix*.

Multiyear Trends and Means. We computed linear least-squares regression slopes of satellite-diagnosed quantities (e.g., EDMS) over time (in decades). Regressions were calculated for the entire study period (1998–2016, $n = 19$ y) and, north of 70°N, for 3 subperiods showing distinct trends. We also calculated mean EDMS during the initial (1998–2003) and final (2011–2016) 6 y, which represent the contiguous years with highest and lowest sea-ice extent, respectively, and without significant trends in sea-ice extent ($P > 0.05$). Division of regression slopes by the mean EDMS during 1998–2003 yielded relative rates of change (% $decade^{-1}$). To compute 19-y trends we checked the coherence between SeaWiFS and MODIS-Aqua records between 2003 and 2007, and corrected for small offsets (<3.5%; Fig. 4*A*) prior to regression analysis.

Uncertainty Assessment. We assessed the sensitivity of EDMS to variations in input satellite products and algorithm configuration (*SI Appendix*, section 5 and Table S3). This analysis was conducted only for the MODIS-Aqua record, which largely drives observed temporal trends. The sensitivity tests included random perturbation of DMS algorithm coefficients, use of alternative Chl products and gas-exchange schemes, and replacement of time-varying DMS fields by climatologies (DMS_{SAT} and L11).

ACKNOWLEDGMENTS. We thank the NASA Ocean Biology Distributed Active Archive Center for access to satellite datasets; the European Centre for Medium-Range Weather Forecasts for access to ERA-Interim; T.S. Bates (NOAA/PMEL) and DMS-GO (COST Action 735) for maintenance of the global sea surface DMS(P) database. We are indebted with colleagues who provided additional DMS data: Sohiko Kameyama, Martine Lizotte, Philippe Tortell, and Tereza Járníkova. We thank Eric Rehm and Maxime Benoît-Gagné for IT support; Betty Croft, Jon Abbatt, Rafel Simó, and Salvador Galí for comments on earlier drafts of the manuscript; and 2 anonymous reviewers for constructive comments. We acknowledge funding from the Canada Excellence Research Chair in Remote Sensing of Canada's New Arctic Frontier (M.B.), the Canada Research Chair on Ocean Biogeochemistry and Climate and an NSERC Discovery Grant Program and Northern Research Supplement Program (M.L.), NETCARE (NSERC Climate Change and Atmospheric Research program) and ArcticNet (The Network of Centres of Excellence of Canada), and AGAUR (Generalitat de Catalunya) Beatriu de Pinós postdoctoral fellowship program (M.G.). This is a contribution to the research program of Québec-Océan and the Takuvik Joint International Laboratory (CNRS-France & Université Laval-Canada).

1. AMAP, *Snow, Water, Ice and Permafrost in the Arctic (SWIPA) 2017* (Arctic Monitoring and Assessment Programme (AMAP), Oslo, Norway, 2017).
2. S. Bélanger, M. Babin, J.-E. Tremblay, Increasing cloudiness in Arctic damps the increase in phytoplankton primary production due to sea ice receding. *Biogeosciences* **10**, 4087–4101 (2013).
3. J. K. Ridley, M. A. Ringer, R. M. Sheward, The transformation of Arctic clouds with warming. *Clim. Change* **139**, 325–337 (2016).
4. K. R. Arrigo, G. L. van Dijken, Secular trends in Arctic Ocean net primary production. *J. Geophys. Res.* **116**, C09011 (2011).
5. M. Vancoppenolle *et al.*, Future Arctic Ocean primary productivity from CMIP5 simulations: Uncertain outcome, but consistent mechanisms. *Global Biogeochem. Cycles* **27**, 605–619 (2013).
6. K. R. Arrigo, G. L. van Dijken, Continued increases in Arctic Ocean primary production. *Prog. Oceanogr.* **136**, 60–70 (2015).

7. P. Wassmann, M. Reigstad, Future Arctic Ocean seasonal ice zones and implications for pelagic-benthic coupling. *Oceanography* **24**, 220–231 (2011).
8. M. Kahru, V. Brotas, M. Manzano-Sarabia, B. G. Mitchell, Are phytoplankton blooms occurring earlier in the Arctic? *Glob. Change Biol.* **17**, 1733–1739 (2011).
9. S. Renaut, E. Devred, M. Babin, Northward expansion and intensification of phytoplankton growth during the early ice-free season in Arctic. *Geophys. Res. Lett.* **45**, 10,590–10,598 (2018).
10. G. Neukermans, L. Oziel, M. Babin, Increased intrusion of warming Atlantic water leads to rapid expansion of temperate phytoplankton in the Arctic. *Glob. Change Biol.* **24**, 2545–2553 (2018).
11. W. K. W. Li, F. A. McLaughlin, C. Lovejoy, E. C. Carmack, Smallest algae thrive as the Arctic Ocean freshens. *Science* **326**, 539 (2009).
12. M. Blais *et al*., Contrasting interannual changes in phytoplankton productivity and community structure in the coastal Canadian Arctic Ocean. *Limnol. Oceanogr.* **62**, 2480–2497 (2017).
13. R. Simó, Production of atmospheric sulfur by oceanic plankton: Biogeochemical, ecological and evolutionary links. *Trends Ecol. Evol.* **16**, 287–294 (2001).
14. M. Levasseur, Impact of Arctic meltdown on the microbial cycling of sulphur. *Nat. Geosci.* **6**, 691–700 (2013).
15. M. Galí, R. Simó, Occurrence and cycling of dimethylated sulfur compounds in the Arctic during summer receding of the ice edge. *Mar. Chem.* **122**, 105–117 (2010).
16. A. Lana *et al*., An updated climatology of surface dimethlysulfide concentrations and emission fluxes in the global ocean. *Global Biogeochem. Cycles* **25**, GB1004 (2011).
17. M. Galí, M. Levasseur, E. Devred, R. Simó, M. Babin, Sea-surface dimethylsulfide (DMS) concentration from satellite data at global and regional scales. *Biogeosciences* **15**, 3497–3519 (2018).
18. S. Becagli *et al*., Relationships linking primary production, sea ice melting, and biogenic aerosol in the Arctic. *Atmos. Environ.* **136**, 1–15 (2016).
19. M. B. Osman *et al*., Industrial-era decline in subarctic Atlantic productivity. *Nature* **569**, 551–555 (2019).
20. S. Wang, S. Elliott, M. Maltrud, P. Cameron-Smith, Influence of explicit *Phaeocystis* parameterizations on the global distribution of marine dimethyl sulfide. *J. Geophys. Res. Biogeosci.*, 10.1002/2015JG003017 (2015).
21. A. J. Gabric, B. Qu, P. Matrai, A. C. Hirst, The simulated response of dimethylsulfide production in the Arctic Ocean to global warming. *Tellus B Chem. Phys. Meterol.* **57**, 391–403 (2005).
22. M. Perrette, A. Yool, G. D. Quartly, E. E. Popova, Near-ubiquity of ice-edge blooms in the Arctic. *Biogeosciences* **8**, 515–524 (2011).
23. W. R. Leaitch *et al*., Dimethyl sulfide control of the clean summertime Arctic aerosol and cloud. *Elem. Sci. Anth.* **1**, 17 (2013).
24. R. Mahmood, K. von Salzen, A.-L. Norman, M. Galí, M. Levasseur, Sensitivity of Arctic sulfate aerosol and clouds to changes in future surface seawater dimethylsulfide concentrations. *Atmos. Chem. Phys.* **19**, 6419–6435 (2019).
25. J. P. D. Abbatt *et al*., Overview paper : New insights into aerosol and climate in the Arctic. *Atmos. Chem. Phys.* **19**, 2527–2560 (2019).
26. J. Browse *et al*., The complex response of Arctic aerosol to sea-ice retreat. *Atmos. Chem. Phys.* **14**, 7543–7557 (2014).
27. M. Dall Osto *et al*., Arctic sea ice melt leads to atmospheric new particle formation. *Sci. Rep.* **7**, 3318 (2017).
28. K.-T. Park *et al*., Observational evidence for the formation of ocean DMS-derived aerosols during Arctic phytoplankton blooms. *Atmos. Chem. Phys.* **17**, 9665–9675 (2017).
29. R. J. Charlson, J. E. Lovelock, M. O. Andreae, S. G. Warren, Oceanic phytoplankton, atmospheric sulphur, cloud albedo and climate. *Nature* **326**, 655–661 (1987).
30. S. Sharma *et al*., Influence of transport and ocean ice extent on biogenic aerosol sulfur in the Arctic atmosphere. *J. Geophys. Res. Atmos.* **117**, D12209 (2012).
31. M. D. Shupe, J. M. Intrieri, Cloud radiative forcing of the Arctic surface: The influence of cloud properties, surface albedo, and solar zenith angle. *J. Clim.* **17**, 616–628 (2004).
32. T. Mauritsen *et al*., An Arctic CCN-limited cloud-aerosol regime. *Atmos. Chem. Phys.* **11**, 165–173 (2011).
33. K. S. Carslaw *et al*., Large contribution of natural aerosols to uncertainty in indirect forcing. *Nature* **503**, 67–71 (2013).
34. M. Galí, DMS emission dataset (latitudes >45N). Zenodo. https://doi.org/10.5281/zenodo.3243967. Deposited 12 June 2019.
35. T. Jarnikova, J. W. Dacey, M. Lizotte, M. Levasseur, P. D. Tortell, The distribution of methylated sulfur compounds, DMS and DMSP, in Canadian Subarctic and Arctic waters during summer 2015. *Biogeosciences* **15**, 2449–2465 (2018).
36. K. T. Park *et al*., Atmospheric DMS in the Arctic Ocean and its relation to phytoplankton biomass. *Global Biogeochem. Cycles*, 10.1002/2017GB005805 (2018).
37. E. L. Mungall *et al*., Dimethyl sulfide in the summertime Arctic atmosphere: Measurements and source sensitivity simulations. *Atmos. Chem. Phys.* **16**, 6665–6680 (2016).
38. K. D. Six *et al*., Global warming amplified by reduced sulphur fluxes as a result of ocean acidification. *Nat. Clim. Chang.* **3**, 975–978 (2013).
39. B. S. Grandey, C. Wang, Enhanced marine sulphur emissions offset global warming and impact rainfall. *Sci. Rep.* **5**, 13055 (2015).
40. Z. Klimont, S. J. Smith, J. Cofala, The last decade of global anthropogenic sulfur dioxide: 2000-2011 emissions. *Environ. Res. Lett.* **8**, 014003 (2013).
41. A. H. Lynch, M. C. Serreze, E. N. Cassano, A. D. Crawford, J. Stroeve, Linkages between Arctic summer circulation regimes and regional sea ice anomalies. *J. Geophys. Res. Atmos.* **121**, 7868–7880 (2016).